Electronic Supplementary Information

Compositional paradigms in multinary compound systems for photovoltaic applications: A case study of kesterites

Andrew Fairbrother, Mirjana Dimitrievska, Yudania Sánchez, Victor Izquierdo-Roca, Alejandro Pérez-Rodríguez, Edgardo Saucedo*

This Electronic Supplementary Information contains additional data about the experimental methods, composition, bandgap, and compositional dependence of optoelectronic properties in $Cu_2ZnSnSe_4$-based solar cells presented in the main text. Specifically, additional compositional maps and the dependence of optoelectronic properties on the commonly reported cationic ratios of Cu/(Zn+Sn) and Zn/Sn is shown. Even though these ratios are more commonly used in describing the composition of kesterite materials, they are less useful in predicting the device performance of devices presented in this work. Because of their common usage they are included here as supplemental information. Some of the figures are directly complementary to Figures 1 and 2 in the main text.

Compositionally graded CZTSe films were prepared by selenization of metallic stack precursors. The DC-magnetron sputtering system (Alliance Ac450) has three off-center sputtering targets, and the substrate is typically rotated during deposition in order to deposit a uniform film. However, to prepare the compositionally graded films, the substrate (10x10 cm^2 Mo-coated soda-lime glass) was not rotated during the sequential deposition of Sn, Cu, and Zn. The resulting Sn/Cu/Zn precursor stack contains a 100-500 nm layer of each metal, depending on the distance of each part of the substrate from the sputter target during deposition, and is then cut into a 5x5 cm^2 sample, taking into account the compositional range of interest. For this study Cu-poor (Cu/(Zn+Sn)<1) and Zn-rich (Zn/Sn>1) compositions were of greatest interest because they correspond to conditions hereto required for the highest efficiency devices, though overlap into stoichiometric, Cu-rich and Zn-poor regions were also investigated. The precursor film is then placed into a graphite box containing elemental Sn (5 mg) and Se (200 mg). The tin acts to minimize Sn-loss from the film during annealing (in the form of $SnSe_2$), and the selenium is to convert the Cu-Zn-Sn stack into $Cu_2ZnSnSe_4$. The graphite box is a semi-closed system which maintains a uniform atmosphere and temperature inside of the container. Annealing took place in a tubular furnace in a two-step process, first for 30 minutes at 450 °C under flowing Ar with a background pressure of 1 mbar, and then for 15 minutes at 550 °C under a constant 1 bar Ar pressure.

Devices were made out of the graded CZTSe film by formation of a CdS buffer layer by chemical bath deposition, and then pulsed DC-magnetron sputtering deposition (Alliance CT100) of a ZnO and ZnO:Al transparent conducting oxide layer. The completed sample (5x5 cm^2) was then mechanically scribed into nearly 200 cells with an area of 3x3 mm^2. In this way, the cells were isolated into regions of relatively constant composition with which to correlate the optoelectronic properties. The sample was then submitted to a soft thermal annealing at 200 °C in air before measuring optoelectronic properties [ref. 23 in main paper]. While data for only one 5x5 cm^2 solar cell sample is presented, another has been prepared, showing the same compositional dependence of optoelectronic properties.

X-ray fluorescence spectroscopy (Fischerscope XVD) mapping measurements were used to determine the composition of the sample before and after annealing, and was previously calibrated to standard samples measured by inductively coupled plasma optical emission spectroscopy (ICP-OES). Raman scattering spectroscopy was used to characterize not only the CZTSe phase, but also detect secondary phases. This was done using a Horiba Jobin Yvon systems LabRam HR800 and T64000 systems under 532 nm and 458 nm excitation conditions respectively. Illuminated AM1.5 current-voltage characteristics were measured for each cell (ABET3000 Solar Simulator), as was external quantum efficiency (Bentham PVE300 characterization system).

In Figure S1 the compositional map of the graded kesterite film with ratios Cu/(Zn+Sn) and Zn/Sn is shown, this is the same sample presented in Figure 1 of the main text which shows the ratios of Cu/Zn and Cu/Sn.

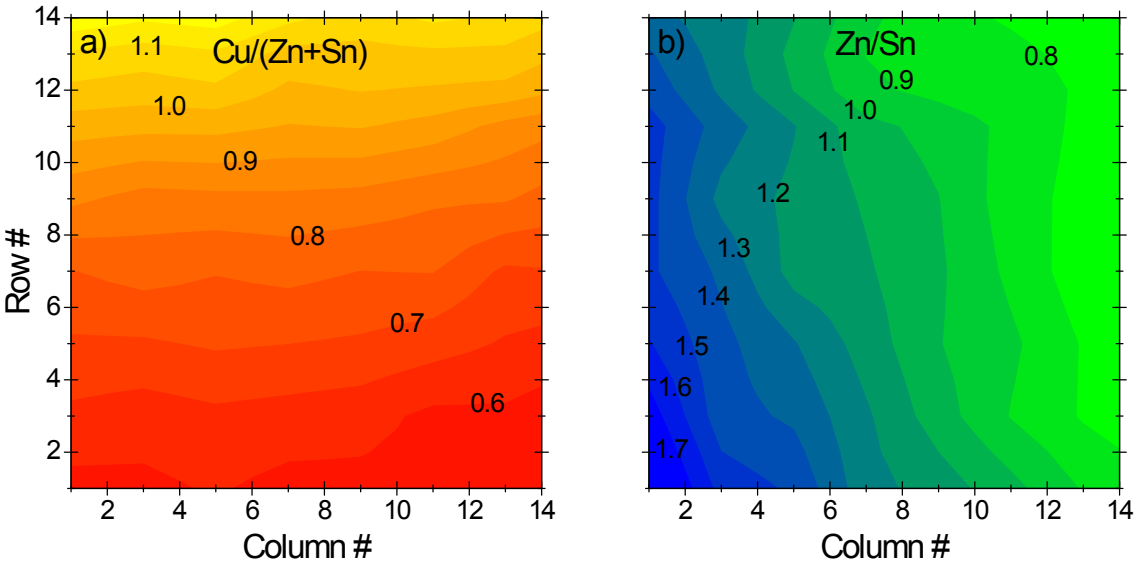

Figure S1. Compositional mapping of the ratios Cu/(Zn+Sn) (left) and Zn/Sn (right) of a 5x5 cm^2 graded kesterite film; each [column,row] corresponds to one 3x3 mm^2 cell.

In addition to power conversion efficiency, open circuit voltage, and short circuit current, another important optoelectronic property is the fill factor (FF), which it is found to have a similar dependence on the cation composition as the V_{OC}. This is shown in Figure S2, presented with dependence on Cu/Zn and Cu/Sn as in Figure 2 in the main text, and has a maximum value of 62%, which is also the highest efficiency and V_{OC} cell.

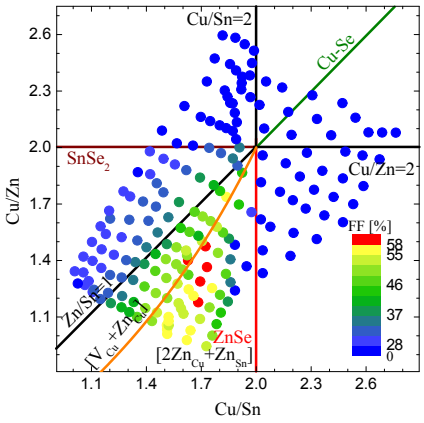

Figure S2. Dependence of FF on Cu/Zn and Cu/Sn for a compositionally graded CZTSe solar cell; lines indicate expected secondary phases or defect clusters for a given region, and stoichiometric cation ratios.

Figure S3 shows the same data as presented in Figure 2 in the main text, but with different cation ratios. It shows the dependence of optoelectronic properties (efficiency, V_{OC}, J_{SC}, and FF) on the ratios of Cu/(Zn+Sn) and Zn/Sn. The trends correspond well with reports on the high efficiency device, namely that the range of Cu/(Zn+Sn) = 0.7-0.9 and Zn/Sn = 1.1-1.4 is ideal for high efficiency devices. However, Cu/Sn is found to be a much stronger indicator of device properties (specifically efficiency, V_{OC} and FF), as discussed in the main text. J_{SC} is the only main property which does correlate strongly with the ratio of Cu/Sn, and in this case the ratio of Zn/Sn has the narrowest range for the highest values (1.1-1.3).

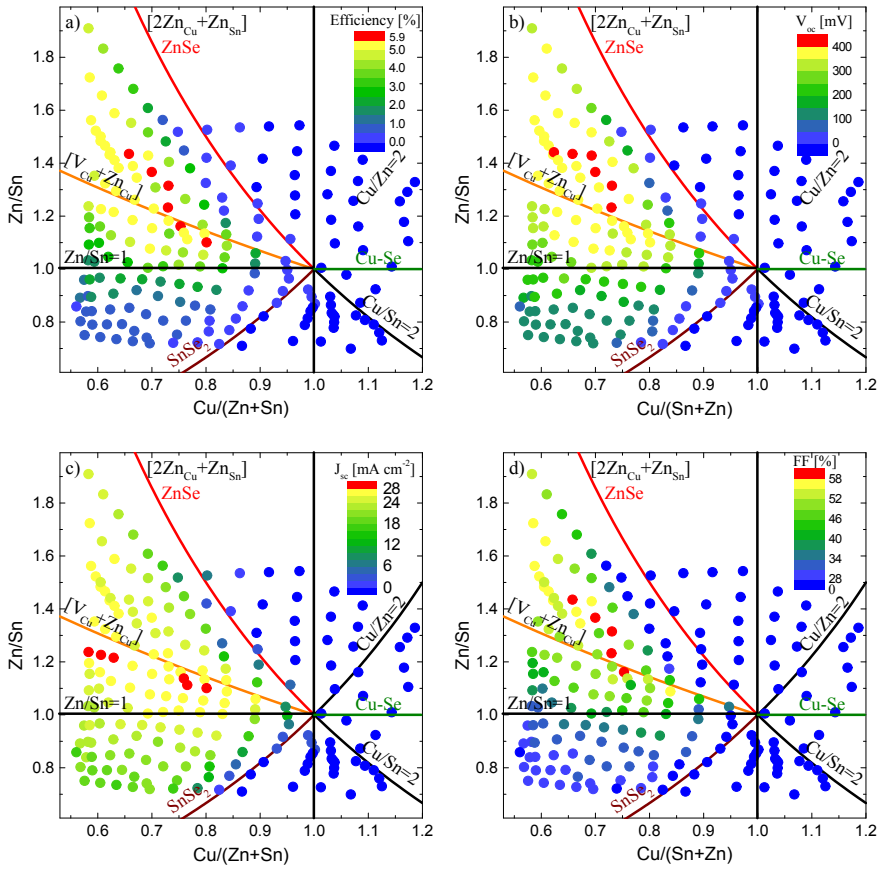

Figure S3. Dependence of optoelectronic properties on composition – efficiency (a), V_{OC} (b), J_{SC} (c), and FF (d) – for Cu/(Zn+Sn) vs. Zn/Sn for a compositionally graded CZTSe solar cell; lines indicate expected secondary phases or defect clusters for a given region, and stoichiometric ratios.

External quantum efficiency was measured in order to estimate the bandgap of each cell by extrapolation of the high wavelength cut-off region. Absorber bandgap has a strong influence on the optoelectronic properties of a device, as exemplified by changes in anion composition of $Cu_2ZnSn(S,Se)_4$ solid-solutions as light absorbers for solar cells. For these materials low bandgap selenium-rich devices have substantially lower V_{OC} and higher J_{SC} compared to high bandgap sulfur-rich devices. Changes in the cation composition have also been shown to influence the bandgap of kesterite compounds, though on a smaller scale, thus one may expect changes in the bandgap from differences in the cation composition to play a similar role. In fact, this is not found to be the case, as shown in Figure S4 which shows the dependence of the estimated bandgap on V_{OC} and J_{SC}. The majority of the high efficiency (>5%) cells have bandgaps in the range of 0.88-0.92 eV. There is a spread of bandgap values in the high V_{OC} and high J_{SC} regions, and it is clear that the highest bandgap cells do not necessarily have the highest V_{OC}, nor do the lowest bandgap cells have the highest J_{SC}. Thus it can be said that changes in the bandgap alone are not responsible for the optimization of these parameters under different compositions, but secondary phases and defect clusters must also be taken into account.

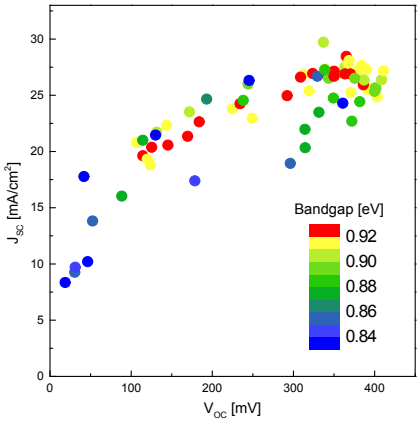

Figure S4. Influence of EQE estimated bandgap on V_{OC} and J_{SC}; contrary to expectation, the highest bandgap cells do not have the highest V_{OC}, nor do the lower bandgap cells have the highest J_{SC}.